Supplementary Information

IL@CQDs catalyzed Active Ester Rearrangement for Detection and Removal of Cyanide Ions

Monika Chaudhary[a‡], Meenakshi Verma[b‡], Pushap Raj[c], K. C. Jena[a,d], Narinder Singh[c,]*

[a]Centre for Biomedical Engineering, Indian institute of Technology Ropar, Roopnagar, Punjab-140001,
[b]Department of UCRD, Chandigarh University, Gharaun, Mohali – 140413, India.
[c]Department of Chemistry, Indian institute of Technology Ropar, Roopnagar, Punjab-140001,
[d]Department of Physics, Indian institute of Technology Ropar, Roopnagar, Punjab-140001,
‡Equal Contribution
*Corresponding author (Narinder Singh) E-mail: nsingh@iitrpr.ac.in; Tel: +91-1881242176.

Table of Contents

Figure S6. XRD pattern of carbon quantum dots showing amorphous morphology.

Figure S7. Structure of the catalysts used for the synthesis, (B) UV- Visible absorption spectra of IL1, IL2, CQDs, IL1@CQDs and IL2@CQDs, (C) Emission profile of IL1, IL2, CQDs, IL1@CQDs and IL2@CQDs, (D) Fluorescence spectra of CQDs at different excitation wavelengths showing excitation dependent emission, (E) HRTEM micrograph of the CQDs exhibiting monodispersity, (F) FT-IR spectra of CQDs (in black line), CQDs coupled with ionic liquid IL1 (red line) and CQDs coupled with ionic liquid IL2 (blue line) , (G) DLS micrograph of the CQDs exhibiting average particle size 8 nm.

Figure S8. DLS histogram of the ionic liquid decorated carbon quantum dots.

Figure S9. Effect of repeated use of **IL2@CQDs** as a catalyst on yield of reaction.

Figure S10. Effect of repeated use of **IL1@CQDs** as a catalyst on yield of reaction.

Figure S11. Effect of pH on compound 2 with and without the addition of cyanide ion.

Figure S12. (a) In visible light colour change of Coated Silica with different anions, (b) Upon illumination with light of 365 nm, emission color change of coated silica. In both a,b 1 = blank host, 2 = CN^-, 3 = F^-, 4 = Cl^-, 5 = Br^-, 6 = I^-, 7 = PO_4^{3-}, 8 = HSO_4^-, 9 = NO_3^-, 10 = CH_3COO^-, 11 = OH^- and 12 = ClO_4^- ions.

Figure S13. (a) Percentage removal of cyanide ions using Flow rate of 1 μM aqueous solution of cyanide; (b) Percentage removal of cyanide ions at various concentrations (1 μM, 10 μM, 50 μM, 100 μM and 500 μM) after passing through assembled cartridge; (c) Percentage removal of cyanide ions after passing cartirage in different volumes(5 mL, 50 mL, 100ml, 250 mL, 500 mL, 750 mL and 1000 mL) of 1 μM concentration; (d) Percentage removal of cyanide ions after passing through assembled cartridge at different pH.

Section S1: Fabrication and Characterisations of CQDs and Ionic Liquid based Catalysts

Section S2: Silica Coating of ONPs

Section S3: Removal of Cyanide ions using ONPs coated silica beads

Table S1. Crystal data and structure refinement for product **2**.

Table S2. Bond Lengths for Product **2**.

Table S3. Bond Angles for Product **2**

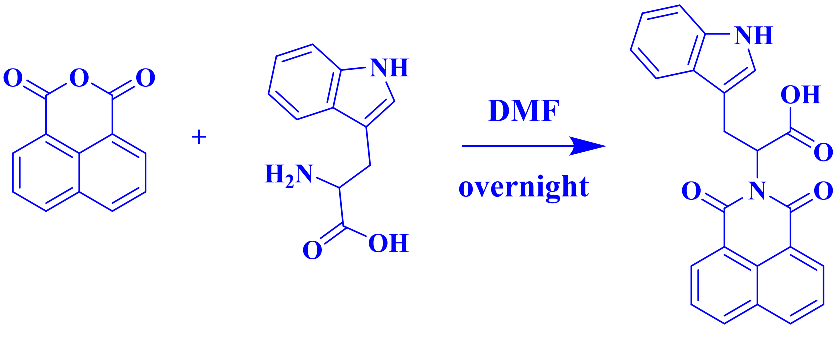

1

Scheme 1. Reaction scheme for the synthesis of amino acid functionalised naphthalimide (product **1**).

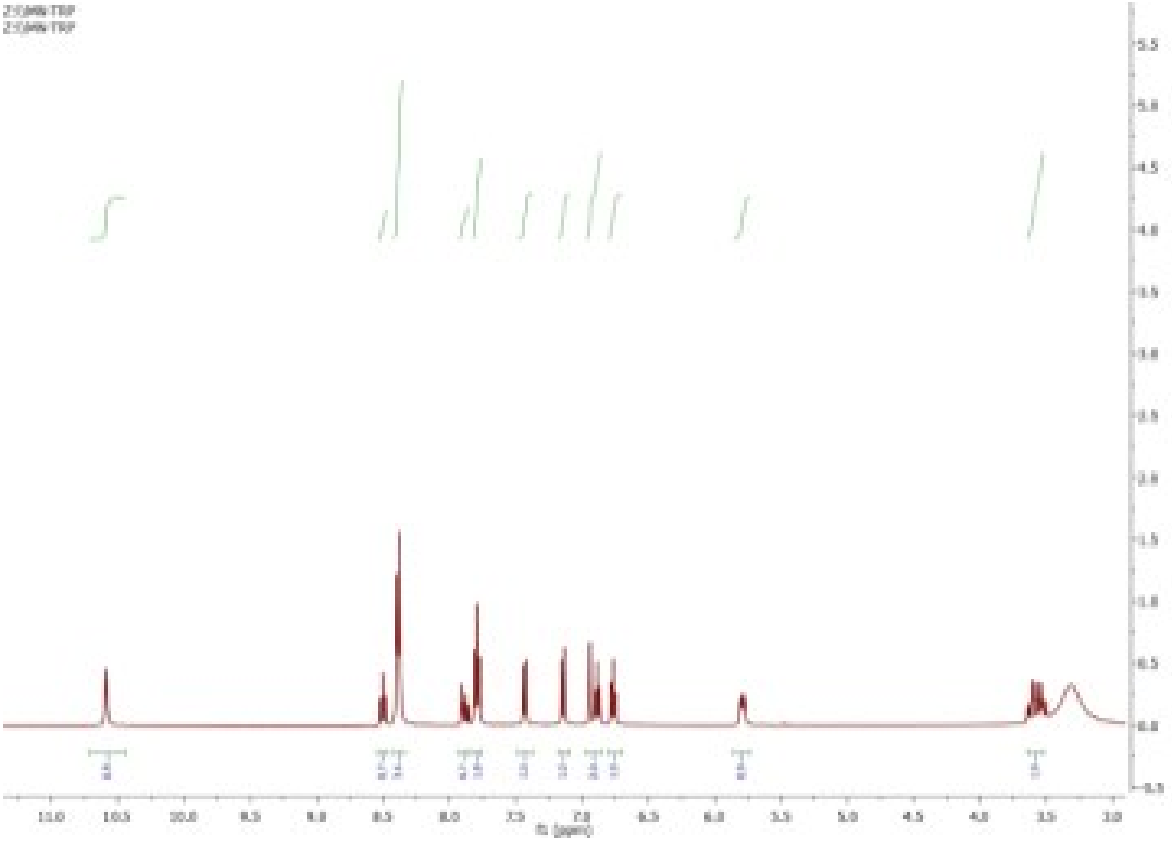

Figure S1. ^{1}H NMR of the product **1**.

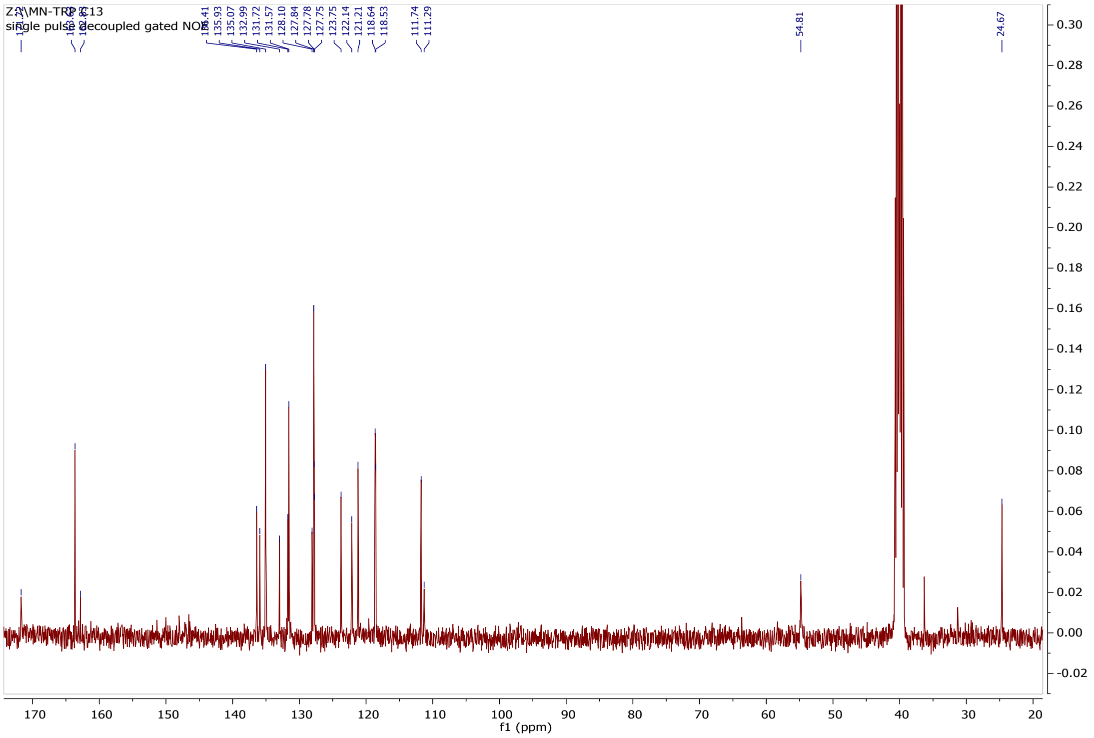

Figure S2. ^{13}C NMR of the product **1**.

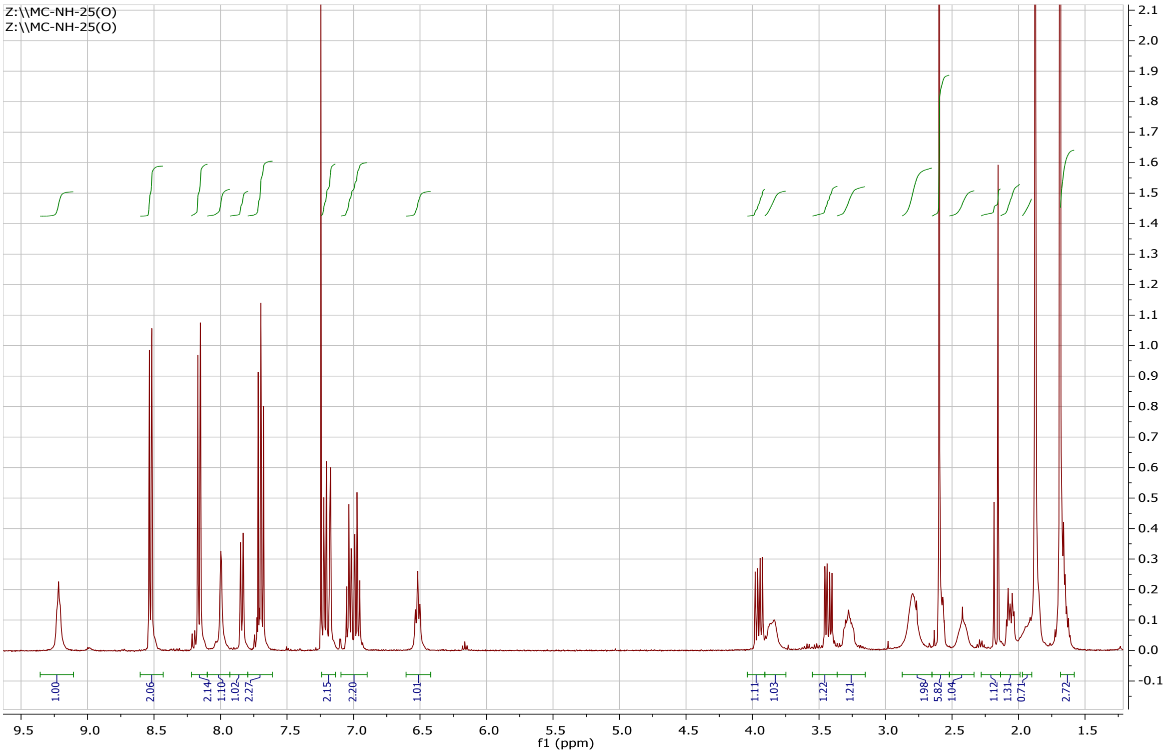

Figure S3. ^{1}H NMR of the product **2**.

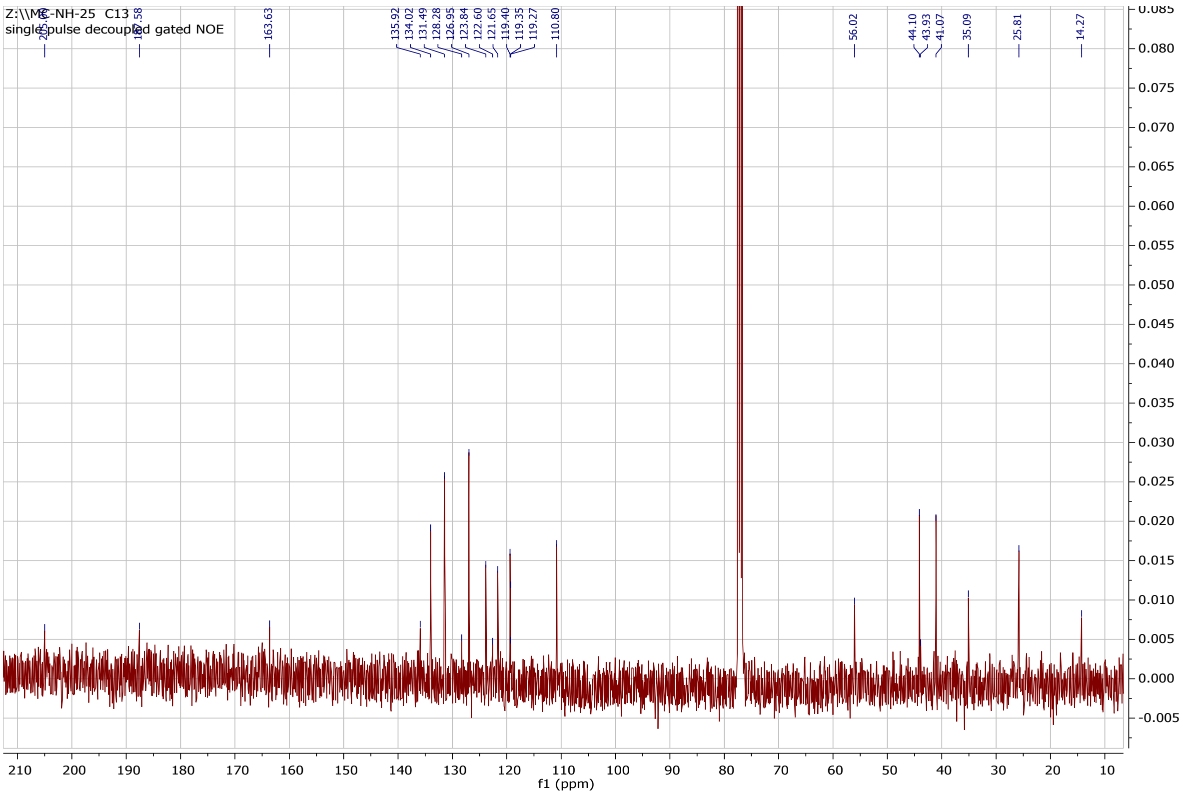

Figure S4. ^{13}C NMR of the product **2**.

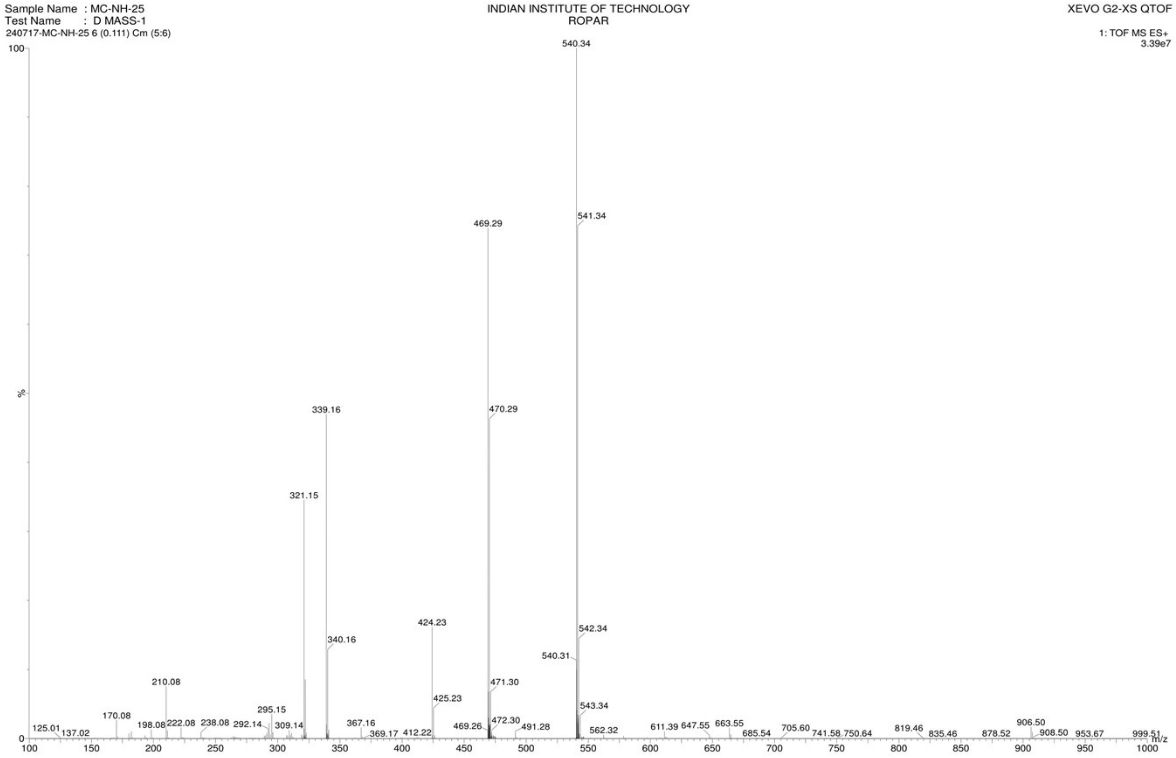

Figure S5. HRMS of the product **2**.

Table S1. Crystal data and structure refinement for product **2**.

Identification code	ns316_01m
Empirical formula	$C_{16.5}H_{20.38}N_{2.5}O_{2.5}S_{0.5}$
Formula weight	309.76
Temperature/K	273.15
Crystal system	triclinic
Space group	P-1
a/Å	8.7663(4)
b/Å	13.3109(7)
c/Å	15.0060(8)
α/°	66.346(2)
β/°	81.935(2)
γ/°	88.778(2)
Volume/Å^3	1586.86(14)
Z	4
ρ_{calc}g/cm^3	1.297
μ/mm^{-1}	0.151
F(000)	660.0
Crystal size/mm^3	3 × 2.6 × 2
Radiation	MoKα (λ = 0.71073)
2Θ range for data collection/°	4.696 to 56.616
Index ranges	$-11 \leq h \leq 11$, $-17 \leq k \leq 17$, $-19 \leq l \leq 19$
Reflections collected	54396
Independent reflections	7860 [R_{int} = 0.1617, R_{sigma} = 0.0651]
Data/restraints/parameters	7860/0/423
Goodness-of-fit on F^2	0.858
Final R indexes [I>=2σ (I)]	R_1 = 0.0699, wR_2 = 0.1895
Final R indexes [all data]	R_1 = 0.1010, wR_2 = 0.2246
Largest diff. peak/hole / e Å^{-3}	0.44/-0.55

Table S2. Bond Lengths for Product **2**

Atom	Atom	Length/Å	Atom	Atom	Length/Å
S1	O5	1.486(3)	N3	C30	1.457(3)
S1	C33	1.781(4)	N5	C21	1.365(3)
S1	C32	1.748(4)	N5	C22	1.372(3)
O1	C1	1.213(2)	C13	C23	1.530(3)
O2	C12	1.213(2)	C6	C5	1.411(4)
N1	C1	1.404(2)	C6	C8	1.408(3)
N1	C12	1.400(2)	C10	C9	1.399(4)
N1	C13	1.476(2)	C17	C18	1.383(3)
O4	C24	1.211(3)	C15	C22	1.356(3)
N2	C23	1.388(3)	C21	C20	1.392(3)
N2	C25	1.476(3)	N4	C27	1.455(3)
N2	C24	1.427(3)	N4	C28	1.448(4)
O3	C23	1.214(2)	N4	C29	1.469(4)
C11	C7	1.406(3)	C25	C26	1.508(4)
C11	C12	1.475(3)	C5	C4	1.362(4)
C11	C10	1.375(3)	C4	C3	1.405(3)
C2	C7	1.413(3)	C19	C18	1.395(4)

C2	C1	1.476(3)	C19	C20	1.367(4)
C2	C3	1.366(3)	O5	S1A	1.269(5)
C7	C6	1.419(3)	C9	C8	1.355(4)
C14	C13	1.540(3)	C26	C27	1.521(4)
C14	C15	1.501(3)	C30	C31	1.411(7)
C16	C17	1.399(3)	C30	C31A	1.401(9)
C16	C15	1.432(3)	C33	S1A	1.679(6)
C16	C21	1.416(3)	C32	S1A	1.783(7)
N3	C24	1.337(3)			

Table S3. Bond Angles for Product **2**

Atom	Atom	Atom	Angle/°	Atom	Atom	Atom	Angle/°
O5	S1	C33	107.57(16)	C8	C6	C5	123.6(2)
O5	S1	C32	107.1(2)	N2	C23	C13	119.30(17)
C32	S1	C33	98.4(2)	O3	C23	N2	120.05(19)
C1	N1	C13	116.90(15)	O3	C23	C13	120.65(19)
C12	N1	C1	124.22(16)	C11	C10	C9	120.3(2)
C12	N1	C13	118.51(16)	C18	C17	C16	118.7(2)
C23	N2	C25	116.11(17)	C16	C15	C14	125.56(19)
C23	N2	C24	122.84(18)	C22	C15	C14	128.1(2)
C24	N2	C25	120.02(18)	C22	C15	C16	106.36(19)
C7	C11	C12	120.26(17)	N5	C21	C16	107.47(19)
C10	C11	C7	120.0(2)	N5	C21	C20	130.5(2)
C10	C11	C12	119.7(2)	C20	C21	C16	122.0(2)
C7	C2	C1	119.78(18)	C27	N4	C29	109.6(2)
C3	C2	C7	120.50(19)	C28	N4	C27	112.8(3)
C3	C2	C1	119.73(19)	C28	N4	C29	110.3(2)
C11	C7	C2	120.92(18)	C15	C22	N5	110.6(2)
C11	C7	C6	119.75(19)	N2	C25	C26	115.3(2)
C2	C7	C6	119.3(2)	O4	C24	N2	122.2(2)
O1	C1	N1	120.33(18)	O4	C24	N3	124.1(2)
O1	C1	C2	122.69(18)	N3	C24	N2	113.62(19)
N1	C1	C2	116.98(16)	C4	C5	C6	121.3(2)
O2	C12	N1	120.00(18)	C5	C4	C3	120.3(2)
O2	C12	C11	123.27(18)	C20	C19	C18	121.6(2)
N1	C12	C11	116.70(17)	C2	C3	C4	120.3(2)
C15	C14	C13	112.78(17)	C17	C18	C19	121.2(2)
C17	C16	C15	134.4(2)	C19	C20	C21	117.7(2)
C17	C16	C21	118.8(2)	C8	C9	C10	120.4(2)
C21	C16	C15	106.85(18)	C9	C8	C6	121.5(2)
C24	N3	C30	121.4(2)	C25	C26	C27	116.2(2)
C21	N5	C22	108.76(19)	N4	C27	C26	114.6(2)
N1	C13	C14	112.55(16)	C31	C30	N3	114.1(3)
N1	C13	C23	111.89(16)	C31A	C30	N3	115.1(5)
C23	C13	C14	111.73(16)	O5	S1A	C33	126.8(5)
C5	C6	C7	118.3(2)	O5	S1A	C32	116.3(4)
C8	C6	C7	118.0(2)	C33	S1A	C32	101.0(3)

Section 1: Fabrication and Characterisations of CQDs and Ionic Liquid based Catalysts

Luminescent CQDs were fabricated from citric acid and ethylenediamine via hydrothermal treatment in Teflon autoclave for 6 hours at 200^{o}C. Prepared CQDs were further functionalized with ionic liquid to improve the feasibility of the reaction. As it is known that ionic liquid serve well in catalysis so the possibility of adding ionic liquid to the CQDs was explored. The ionic liquids IL1 and IL2 were synthesized from nucleophillic substitution of bromoacetic acid with 1 methyl imidazole and benzimidazole as shown in Scheme S2. These synthesized ionic liquids were covalently linked to the CQDs (IL1@CQD and IL2@CQD) in presence of coupling reagents EDC and DMAP for 24 hours (Scheme S2).

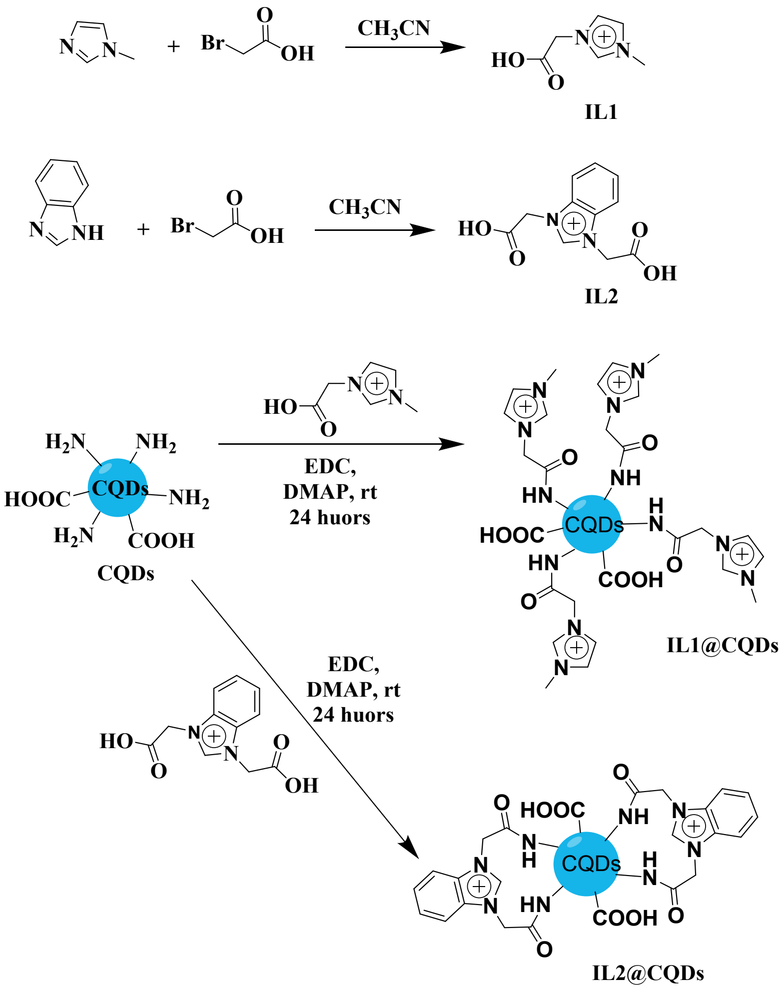

Scheme S2. Schematic diagram of functionalization of carbon quantum dots for usage in catalysis

The structure of the ionic liquids, CQDs and functionalised CQDs used for catalysis are shown in Fig. S7A. The UV – visible absorption spectra of the CQDs were obtained which constitute two absorption bands at 240 nm and 346 nm corresponding to $\pi-\pi^*$and $n-\pi^*$ transitions, respectively. The absorbance band of the IL1 and IL2 is observed at 347 nm corresponding to $\pi-\pi^*$. Ionic liquids coated CQDs shows absorbance at 354 nm (Fig. S7B). The fluorescence spectra were recorded for the ionic liquids, CQDs and ionic liquid coated CQDs (Fig. S7C). The functionalization of the carbon dots with the ionic liquid is clearly visible from the fluorescence graph in which both IL1@CQDs and IL2@CQDs has shown two emission bands one at 400 nm and 450-460 nm when excited at 350 nm. Further, excitation dependent emission was observed in case of CQDs in aqueous medium. The emission profile of the CQDs was recorded at varied wavelengths i.e. from 360 nm to 450 nm (Fig. S7D) As the excitation wavelength was increased; red shift was observed in the emission wavelength along with the quenching of fluorescence intensity. The mechanism behind such process is still unknown and many possibilities have been put forward for this process.[1] Some literature reports suggest that this is attributed to the small size of the particles and there quantum confinement effect.[2,3] Furthermore others suggest that during carbonisation the ratio of sp^3/sp^2 hybridisation changes which results in formation of hole-pair that explains the luminescence behaviour of these CQDs. The HRTEM micrograph reveals the spherical structure of the CQDs having size less than 10 nm and monodisperse dots in water (Fig. S7E). The average particle size was found to be 8 nm which was obtained from particle size analyzer (Fig. S7G). A broad peak was observed at 20^{o} in the XRD pattern of CQDs which shows the disordered structure of the material as shown in literature reports as well (Fig. S6).

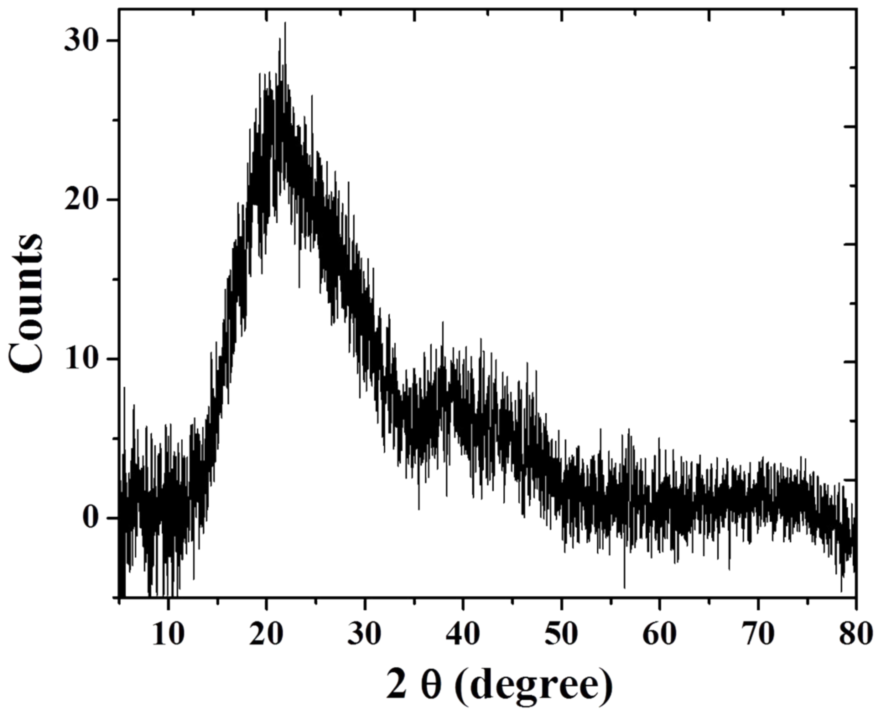

Figure S6. XRD pattern of carbon quantum dots showing amorphous morphology.

The characterisation of the functional groups on the CQDs was performed using Fourier transform infrared (FTIR) spectroscopy (Fig. S7F). The FTIR spectrum is shown below and has been modified in figure. The undecorated CQDs of shows vibrational band at 1350 cm^{-1} correspond to – CH_2 corresponding to alkyl rocking of the carbon quantum dots.[4] The vibration band at 1540 cm^{-1} is coming from the surface –NH_2 groups of the carbon quantum dots.[5] The band at 1640 cm-1 is attributed to the –C=N stretching vibrations and intense band at 1690 cm^{-1} belongs to the carbonyl groups of the carbon quantum dots. A broad band in the range of 3200 – 3400 cm^{-1} is attributed to hydroxyl and amine group stretching vibrations.[6] The FTIR spectroscopy was utilized as a characterization tool to confirm if the ionic liquids have successfully decorated on the surface of the carbon quantum dots through amide coupling. We observed a vibrational peak at 2940 cm^{-1} for IL1@CQDs and IL2@CQDs which corresponds to –CH_2 stretching of the surface functionalized groups of CQDs. Another feature at 3363 cm^{-1} signifies the –NH stretching of the amide bonding which provides evidence of the amide coupling process of the amine of CQDs with –COOH of the ionic liquids.[4] Also the reduction in vibrational band at 3200 – 3500 cm^{-1} signifies that the free –NH_2 is not anymore available but is bonded through amide linkage. These results significantly show the decorations of the ionic liquids on the surface of CQDs. The average particle size analysis was performed with external probe feature of particle size analyzer which shows that on functionalization of the CQDs the average size increases. For as synthesized CQDs, the particle size was 8 nm. However, on functionalization it rises up to 13-17 nm range that proves the achievement of the functionalization of the CQDs at the surface with ionic liquids (Fig. S8).

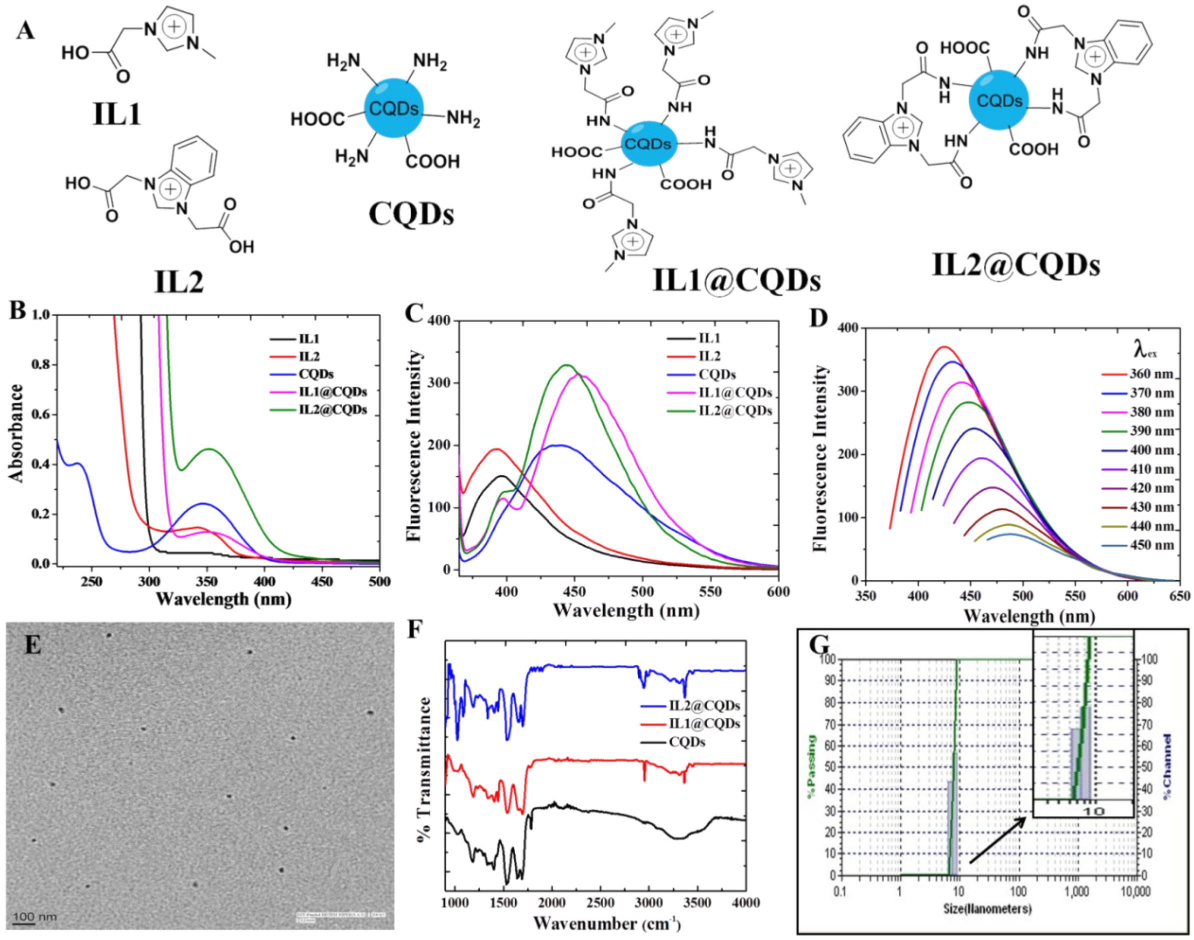

Figure 7. (A) Structure of the catalysts used for the synthesis, (B) UV- Visible absorption spectra of IL1, IL2, CQDs, IL1@CQDs and IL2@CQDs, (C) Emission profile of IL1, IL2, CQDs, IL1@CQDs and IL2@CQDs, (D) Fluorescence spectra of CQDs at different excitation wavelengths showing excitation dependent emission, (E) HRTEM micrograph of the CQDs exhibiting monodispersity, (F) FT-IR spectra of CQDs (in black line), CQDs coupled with ionic liquid IL1 (red line) and CQDs coupled with ionic liquid IL2 (blue line) , (G) DLS micrograph of the CQDs exhibiting average particle size 8 nm.

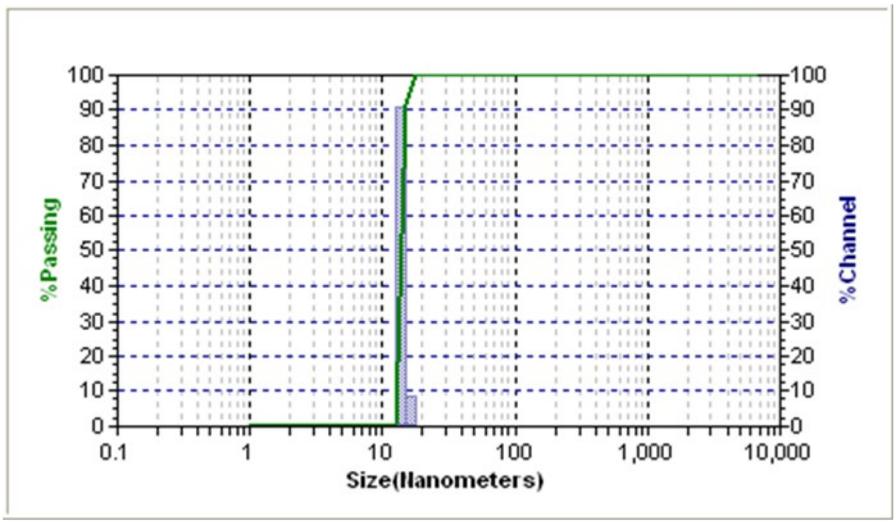

Figure S8. DLS histogram of the ionic liquid decorated carbon quantum dots exhibiting average size 15 nm.

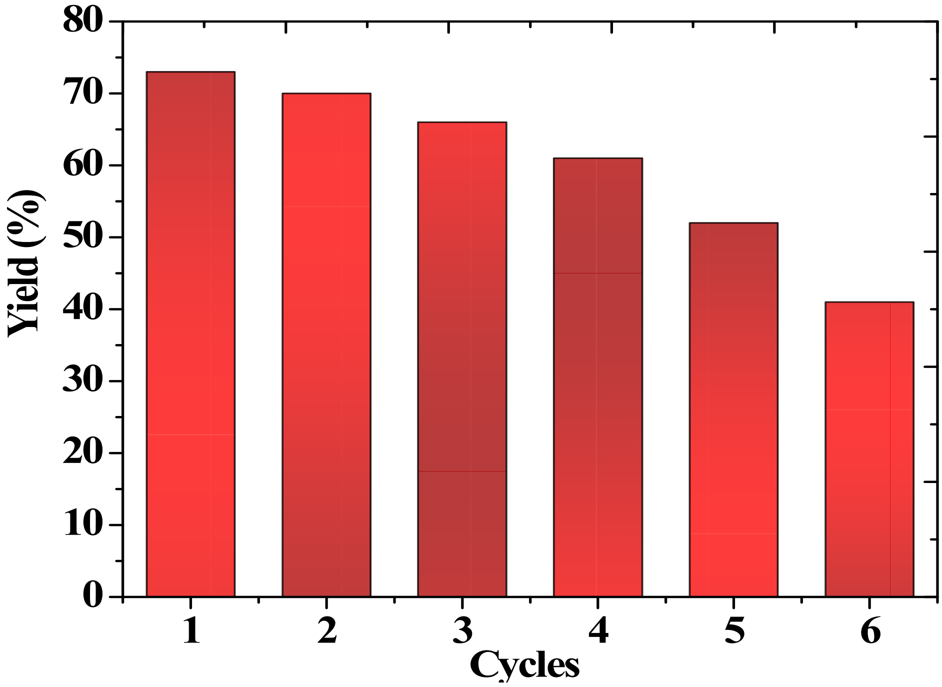

Figure S9. Effect of repeated use of **IL2@CQDs** as a catalyst on yield of reaction.

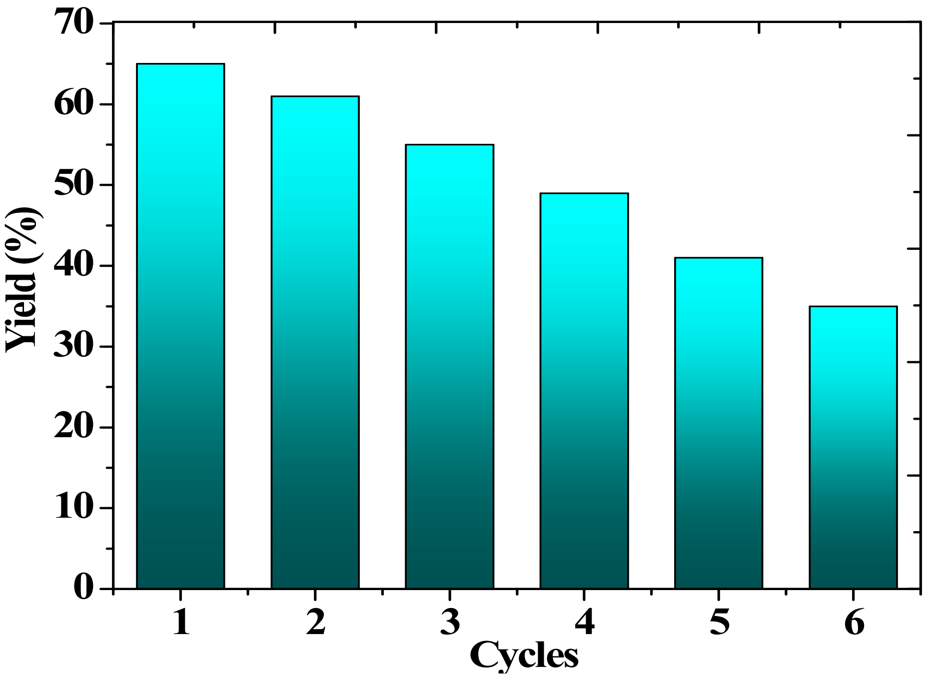

Figure S10. Effect of repeated use of **IL1@CQDs** as a catalyst on yield of reaction.

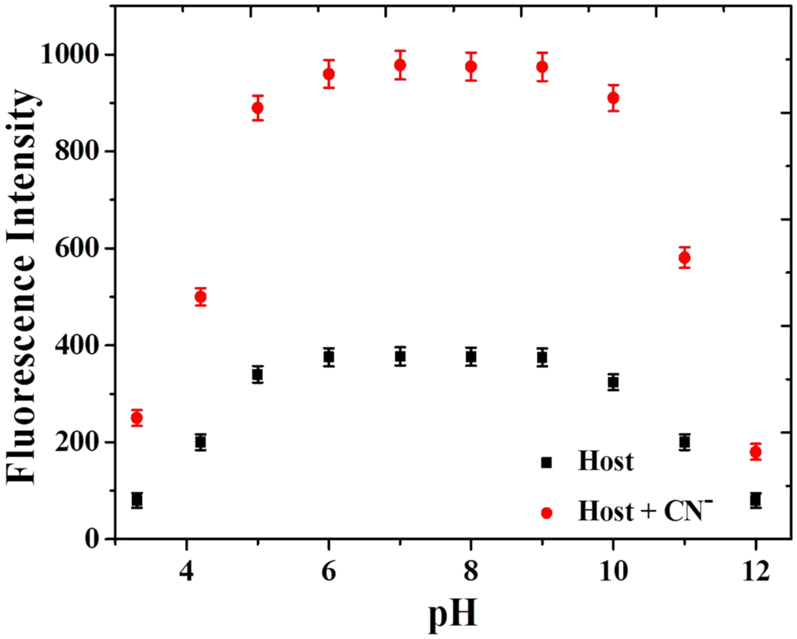

Figure S11. Effect of pH on ONPs with and without the addition of cyanide ion.

Section S2: Silica Coating of ONPs

The organic nanoparticles of the host have been coated on silica beads. Then these coated silica beads have been investigated for its cyanide sensing and removal in solid state. Coating of the ONPs over silica beads was carried out as per the documented literature.[7] The obtained ONPs coated silica beads were then investigated with various anions. Different anions were incubated for two hours with ONPs coated silica beads and changes in the material were observed. As shown in figure S11a, in visible light again no significant changes were observed. In UV light we observe that with CN- the there is visible enhancement in the fluorescence as compared to the rest of the anions as shown in figure S11b. Thus the solid state experiment is in harmony with the solution state experiments.

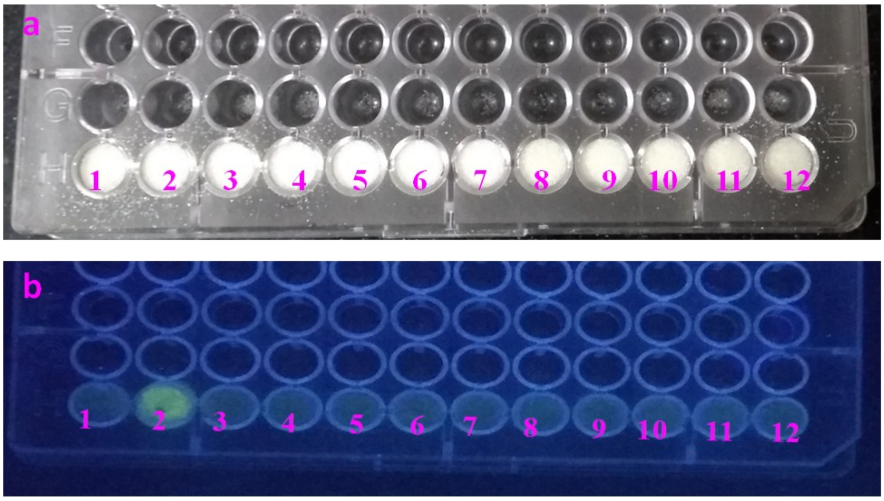

Figure S12. (a) In visible light colour change of Coated Silica with different anions, (b) Upon illumination with light of 365 nm, emission color change of coated silica. In both a,b 1 = blank host, 2 = CN^-, 3 = F^-, 4 = Cl^-, 5 = Br^-, 6 = I^-, 7 = PO_4^{3-}, 8 = HSO_4^-, 9 = NO_3^-, 10 = CH_3COO^-, 11 = OH^- and 12 = ClO_4^- ions.

Section S3: Removal of Cyanide ions using ONPs coated silica beads

We have used ONPs coated silica beads based cartridge device which has been previously described by our group.[8] 5g of ONPs coated silica beads were taken to assemble a cartirage. The flow rate was varied to monitor the efficiency of the process as shown in figure S12a, at 1ml per 10 minutes the percentage removal was maximum (76%), for 10 ml/10 mins the removal was 69% and it decreases with increase in the flow rate. Percentage removal of cyanide ions at various concentrations (1 µM, 10 µM, 50 µM, 100 µM and 500 µM) after passing through assembled cartridge was found to be 71%, 46%, 31%, 25% and 13% respectively as shown in figure S12a. Similar results were obtained for variation in when the flow rate and concentration was kept constant, on increasing the volume the percentage removal lessens as shown in figure S12c. Finally the removal capability of the cartridge was investigated at different pH solution as shown in figure S12d. In acidic pH the removal capacity was low, however the removal capacity was maximum 6-10 and then when go to basic pH the percentage removal reduces. The results of these experiment suggest that this sensor can be successfully used to purify the cyanide impurities from water using ONPs coated silica beads in real samples as well.

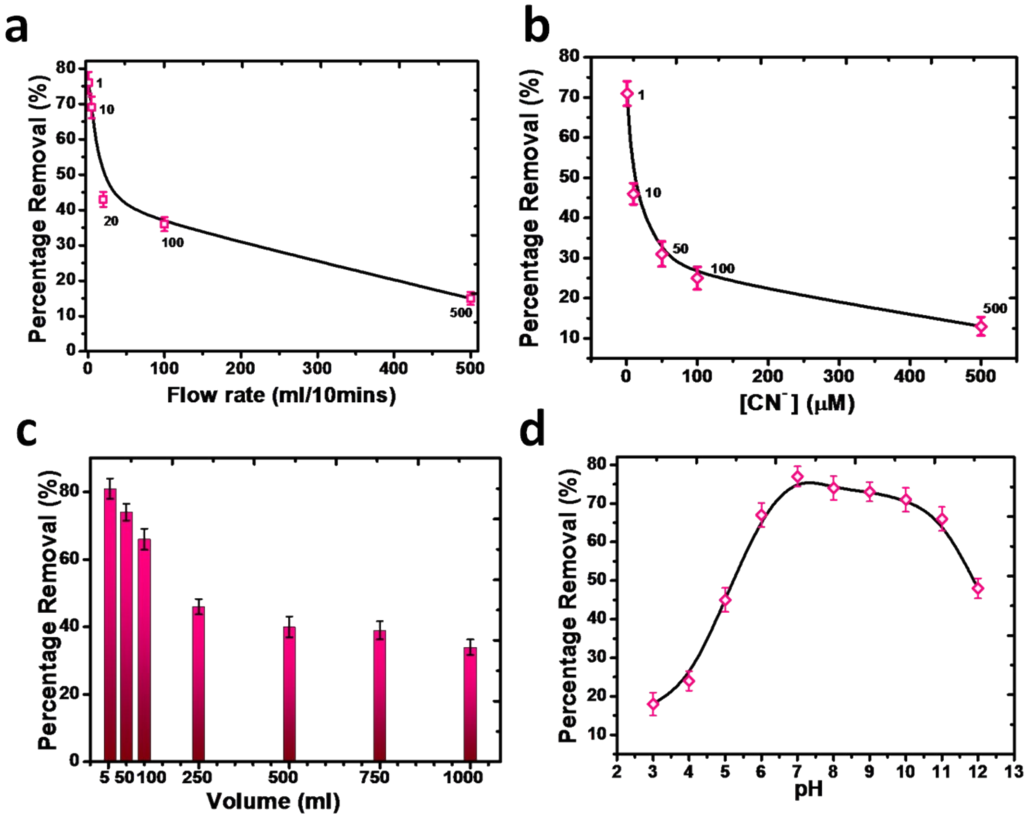

Figure S13. (a) Percentage removal of cyanide ions using Flow rate of 1 μM aqueous solution of cyanide; (b) Percentage removal of cyanide ions at various concentrations (1 μM, 10 μM, 50 μM, 100 μM and 500 μM) after passing through assembled cartridge; (c) Percentage removal of cyanide ions after passing cartirage in different volumes(5 mL, 50 mL, 100ml, 250 mL, 500 mL, 750 mL and 1000 mL) of 1 μM concentration; (d) Percentage removal of cyanide ions after passing through assembled cartridge at different pH.

References:

1. S. Y. Lim, W. Shen and Z. Gao, *Chemical Society Reviews*, 2015, **44**, 362-381.
2. H. Li, X. He, Z. Kang, H. Huang, Y. Liu, J. Liu, S. Lian, C. H. A. Tsang, X. Yang and S. T. Lee, *Angewandte Chemie International Edition*, 2010, **49**, 4430-4434.
3. G. Oza, M. Ravichandran, V.-I. Merupo, S. Shinde, A. Mewada, J. T. Ramirez, S. Velumani, M. Sharon and M. Sharon, *Scientific reports*, 2016, **6**, 21286.
4. A. Cayuela, C. Carrillo-Carrión, M. L. Soriano, W. J. Parak and M. Valcárcel, *Analytical chemistry*, 2016, **88**, 3178-3185.
5. T. Feng, X. Ai, G. An, P. Yang and Y. Zhao, *ACS nano*, 2016, **10**, 4410-4420.
6. Z. Qian, X. Shan, L. Chai, J. Ma, J. Chen and H. Feng, *ACS applied materials & interfaces*, 2014, **6**, 6797-6805.
7. K. L. Solis, G. U. Nam, Y. Hong, *Environ. Eng. Res*. 2016, **21**, 99-107.
8. R. Rani, Mayank, P. Thangarasu, N. Singh, *ACS Applied Nano Materials,* 2018, **2** (1), 1-5.